Coupling and near-field simulations of ion-cyclotron antennas: Numerical validation of the perfectly matched layer technique for several density profiles

Cite as: AIP Conference Proceedings **2254**, 050004 (2020); https://doi.org/10.1063/5.0014864
Published Online: 16 September 2020

S. Ceccuzzi, A. Cardinali, G. L. Ravera, et al.

Coupling and Near-Field Simulations of Ion-Cyclotron Antennas: Numerical Validation of the Perfectly Matched Layer Technique for Several Density Profiles

S. Ceccuzzi[1,a)], A. Cardinali[1], G.L. Ravera[1] and A.A. Tuccillo[1]

[1]*ENEA, C.R. Frascati, Via E. Fermi 45 00044 Frascati (RM), Italy.*

[a)]Corresponding author: silvio.ceccuzzi@enea.it

Abstract. A simplified, flat, plasma-loaded, ion-cyclotron antenna has been simulated using three different modeling approaches and a comparison of simulation outputs is presented in this paper. Several plasma profiles with different density gradients and distances between the antenna and the cutoff density have been used as benchmark for the numerical simulations, which have been run at 30 MHz by means of two tools. The one is the TOrino Polythecnic Ion-Cyclotron Antenna (TOPICA) code that has been repeatedly used and validated for this type of problems. The other tool is the finite-element method (FEM) of a commercial software, where inhomogeneous anisotropic materials can be defined and the perfectly matched layer technique can be adopted. In this tool, two models of antenna load have been implemented: an equivalent dielectric, locally matching the perpendicular propagation constant of the fast wave in the plasma, and a cold plasma model. The simulation results by such models are compared with the results by TOPICA, which relies on a 1-D inhomogeneous, hot plasma.

INTRODUCTION

Waves in the Ion-Cyclotron Range of Frequency (ICRF) have been effectively used in tokamak plasmas for ion or electron heating as well as for many other applications beyond heating [1, 2]. Almost all existing tokamaks use ICRF heating and current drive, and ICRF systems are planned in future machines like ITER and the Italian Divertor Tokamak Test (DTT) facility [3, 4]. ICRF waves are launched through grounded metal stripes, called straps, placed in a recessed antenna box, protected by a Faraday screen made of toroidally aligned metal rods. The electromagnetic problem of plasma facing antennas is formally known, but its full-wave solution is computationally demanding, so simulation tools often introduce some approximations in the modeling of antennas and plasmas. Several tools have been developed, validated, and then employed for both antenna design and predictive or interpretative modeling of ICRF-operated experiments [5, 6, 7]. The antenna load is sometimes modeled with an isotropic dielectric load emulating the plasma behaviour for the fast wave [8]. Such approximation is mostly used to speed up simulations when optimising an antenna design in terms of coupling [9, 10]. More rigorous approaches have been developed too, e.g., finite-element method (FEM) packages [11], time-domain solvers [12] and antenna-to-core integrated modeling [13].

Among plasma-facing ICRF antenna tools, FEM approaches with perfectly matched layer (PML) technique have received particular attention [14, 15] in the last years. They allow the accurate description of realistic antenna geometries along with electromagnetic bandgap materials [16, 17] and modeling of 3-D inhomogeneous cold plasmas [18], which is an attractive feature in view of DTT owing to its several magnetic configurations [19]. In a pioneering work [14], the PML technique was benchmarked with the TOrino Polythecnic Ion-Cyclotron Antenna (TOPICA) code [20], which is well assessed, widely used tool, based on different numerical method and plasma model from the FEM approach. In that comparison a difference by a factor 1.2÷1.5 was found in predicted coupling resistances, but TOPICA antenna model was more detailed, so the cause of the small disagreement could not be ascribed to either tool formulation or differences in geometrical models. Here the two codes are accurately compared at 30 MHz against an identical, simplified, flat, antenna model and several plasma profiles. The latter differ in density gradient and distance between cutoff density and antenna front face, similarly to the density profiles of the sensitivity study documented in [21]. Furthermore an equivalent dielectric have been derived for each profile and simulated in front of the same test

23rd Topical Conference on Radiofrequency Power in Plasmas
AIP Conf. Proc. 2254, 050004-1–050004-4; https://doi.org/10.1063/5.0014864
Published by AIP Publishing. 978-0-7354-2013-7/$30.00

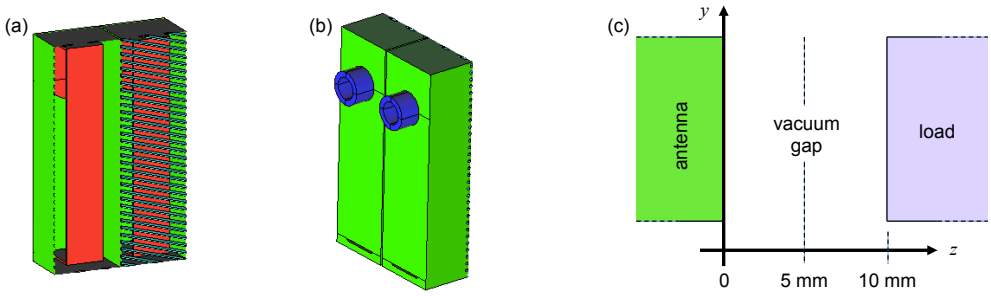

FIGURE 1. Front (a) and back (b) perspective views of the antenna model; One half of the Faraday screen has been removed to make the interior visible. (c) Poloidal section of the geometry with the radial coordinate where electric fields have been computed.

antenna to check the validity of such approximation against the simulation results with plasma.

BENCHMARK SETUP

The reference test geometry is a two-strap antenna without limiters, fed by two coaxial cables with characteristic impedance of 25 Ω. A vacuum layer of 10 mm has been inserted between the antenna and the load, and the electric fields are calculated over a midplane of this vacuum gap. Figure 1 shows the geometrical model.

Nine scenarios that differ in density profile have been considered in front of the antenna. They are based on Deuterium plasma with 3% Hydrogen minority and share the following parameters: major radius $R = 1.65$ m, minor radius $a = 0.5$ m, and magnetic field on axis $B = 2$ T. In this comparison, no tilt has been set for the magnetic field with respect to the equatorial plane. The kinetic profiles have been generated analytically and named with a number and a letter, which identify different clearances and density gradients, respectively. Their plots are given in Fig. 2.

The antenna simulations in such scenarios have been run with the following tools and plasma models:

TOPICA with hot plasma. The TOPICA code is among the most advanced ICRF antenna tools. The electromagnetic problem is formulated by a set of multiple coupled integral equations, enforcing field continuity at the interface between antenna and plasma regions. Such interface along with metal surfaces in the antenna region is discretized with triangular facets as typical for boundary element methods. A sparse algebraic system is finally derived applying a hybrid spatial-spectral method of moments. TOPICA is coupled with FELICE [22] that solves the finite Larmor radius wave equations in a slab plasma model; temperature profiles for all species are thus needed. The low-density portion of the kinetic profiles has been replaced with vacuum to avoid the $S = 0$ resonance.

FEM with cold plasma. Finite element methods are numerical full-wave solvers of partial differential equations. The geometry is usually discretised with tetrahedral elements where the unknown functions are expressed as a linear combination of basis functions. The electromagnetic FEM solvers of the most widespread commercial softwares allow the modeling of inhomogeneous, anisotropic, dispersive materials. A cold plasma

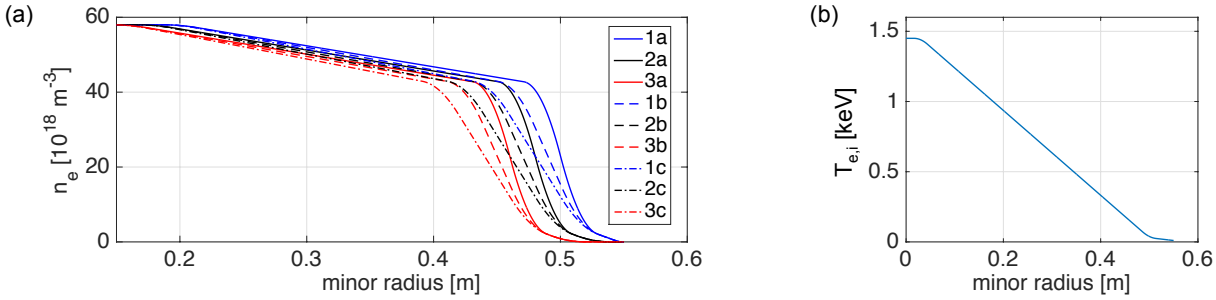

FIGURE 2. Kinetic profiles of the simulations: (a) electron density, (b) electron and ion temperature.

has been modelled by defining a material whose dielectric constant is given by a 1-D inhomogeneous Stix tensor; for convenience the toroidal direction has been aligned with the x-axis, giving

$$\underline{\underline{\epsilon}} = \begin{bmatrix} P & 0 & 0 \\ 0 & S & -iD \\ 0 & iD & S \end{bmatrix} \tag{1}$$

The boundary conditions of outward radiation have been implemented through user-defined PMLs and the low-density portion of the kinetic profiles has been replaced once more with vacuum to avoid the $S = 0$ resonance.

FEM with equivalent dielectric. An isotropic material mimicking the behaviour of a plasma load has been modeled with the same FEM tool. This material is a 1-D inhomogeneous equivalent dielectric, locally matching the perpendicular propagation constant of the fast wave in the plasma. Several expressions for the equivalent dielectric constant have been proposed in literature [23]; here the following has been adopted [8]:

$$\epsilon = S - \frac{D^2}{S - n_{\parallel}^2} \tag{2}$$

where the peak parallel refractive index has been used for $n_{\parallel}$. The boundary conditions of outward radiation have been implemented with software-defined PMLs.

A structured mesh with maximum element size of around $\lambda/5$ in radial direction, being λ the wavelength in the propagating medium, has been enforced in the load of FEM models, while relaxing element size toroidally and poloidally with the scaling factors reported in [14]. A free tetrahedral mesh, i.e., automatically defined by the software, has been used in the antenna domain, making it slightly denser in the coaxial feeders. Widely used discretisation settings have been also used in FELICE (radial steps of 1 cm) and TOPICA (maximum element size of 4 cm). An extensive set of simulations proved that such settings are rather general and work well for most ICRH antennas and plasmas, so adaptive mesh refinement has not been performed. The order of basis functions cannot be varied in TOPICA that relies on Rao–Wilton–Glisson functions. For FEM convergence, quadratic functions have been used since the use of cubic ones gave a negligible variation of results.

COMPARISON OF RESULTS

The comparison between aforementioned modeling approaches has been carried out in terms of circuit network parameters, electric fields and radiated power spectra, setting a 0π phase difference between feeder inputs, i.e., dipole phasing. Good agreement has been found with reference to power spectra, mostly between TOPICA and the FEM code with cold plasma. This comparison is not plotted here for the sake of brevity. For the same reason, global figures of merit are only used here. Alternative approaches of code verification could be adopted, e.g., by comparing the terms of scattering matrices in place of the coupled power or electric field maps rather than RF potentials. To assess the role played by plasma model more in detail, a comparison of the plasma surface admittance can be envisaged too.

Concerning the antenna electrical parameters, the coupled power has been used as term of comparison according to the following definition

$$\text{Coupled power} = \frac{V_{\max}^2}{2Z_c} \sum_{i=1}^{2} \frac{1}{VSWR_i} \tag{3}$$

where $V_{\max} = 30$ kV is the considered standoff voltage, $Zc = 30\ \Omega$ is the feeder characteristic impedance, and $VSWR_i$ is the voltage standing wave ratio of the ith feeder. The latter is derived from the antenna scattering matrices computed by the tools for each scenario.

As regards the electric fields, the average value of RF potentials, computed at the middle of the vacuum layer (see Fig. 1) and normalized to a coupled power of 1.5 MW, have been compared. In this work the RF potentials have been calculated as the integrals of $|E_{\parallel}|$ along the magnetic field lines of the tokamak, being $E_{\parallel}$ the electric field component parallel to the equilibrium magnetic field. The calculation of RF potentials is very sensitive to the geometry discretisation, so a similar mesh has been set in all models at the plane where electric fields are computed.

The two figures of merit are compared in Fig. 3 for all scenarios, showing a good agreement between the three approaches with reference to the predictions of coupled power. As fas as RF potentials are concerned, only results

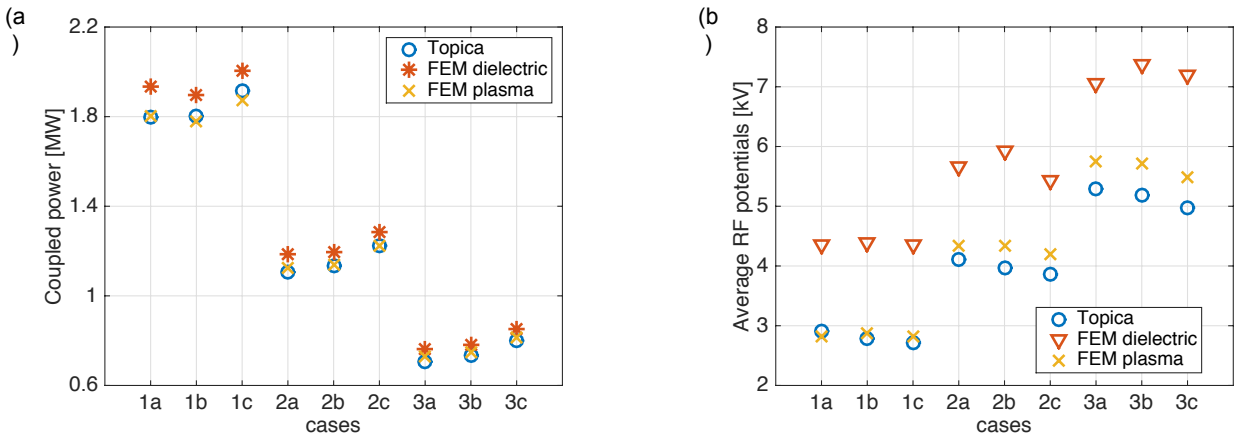

FIGURE 3. Predicted coupled power (a) and maximum RF potentials (b) for all density profiles of Fig. 2.

obtained with either hot or cold plasma model show an acceptable match, whereas the approach with the equivalent dielectric gives rather different predictions. Clearly the latter does not take into account the slow wave, thus giving a different field matching condition at the vacuum–load interface. Apart from this, another important difference is that the equivalent dielectric constant always starts at such interface, whereas in the other approaches the vacuum layer is extended up to the $S = 0$ resonance, so its effective depth depends on the density profile.

CONCLUSIONS

A test antenna in front of several plasma profiles has been simulated with TOPICA and a FEM code with the PML technique. In the latter the antenna load has been modeled with either a cold plasma or an equivalent dielectric. A very good agreement has been found for the predictions of the coupling performance. With respect to RF potentials, plasma modeling by an equivalent dielectric has been shown to give different results from the other modeling approaches, which instead agree with each other, provided that a similar mesh is set in the geometrical models.

REFERENCES

1. A. Becoulet, Plasma Physics and Controlled Fusion **38**, A1–A11 (1996).
2. M. J. Mantsinen *et al.*, Plasma Physics and Controlled Fusion **45**, A445–A456 (2003).
3. F. Durodié *et al.*, AIP Conference Proceedings **1580**, 362–365 (2014).
4. G. Granucci *et al.*, Fusion Engineering and Design **122**, 349–355 (2017).
5. C. Qin, Y. Zhao, L. Colas, and S. Heuraux, AIP Conference Proceedings **933**, 183–186 (2007).
6. S. Ceccuzzi *et al.*, Int. Journal on Applied Electromagnetics and Mechanics **39**, 59–64 (2012).
7. W. Zhang *et al.*, Plasma Physics and Controlled Fusion **59**, p. 075004 (2017).
8. A. Messiaen *et al.*, Fusion Engineering and Design **86**, 855–859 (2011).
9. F. Louche, P. Dumortier, A. Messiaen, and F. Durodié, Nuclear Fusion **51**, p. 103002 (2011).
10. S. Ceccuzzi *et al.*, Fusion Engineering and Design (2018), 10.1016/j.fusengdes.2018.12.068.
11. S. Shiraiwa *et al.*, Physics of Plasmas **17**, p. 056119 (2010).
12. Jenkins, Thomas G. and Smithe, David N., EPJ Web Conf. **157**, p. 03021 (2017).
13. Wright, J. and Shiraiwa, S., EPJ Web Conf. **157**, p. 02011 (2017).
14. J. Jacquot *et al.*, Plasma Physics and Controlled Fusion **55**, p. 115004 (2013).
15. L. Colas *et al.*, Journal of Computational Physics **389**, 94 – 110 (2019).
16. D. Milanesio and R. Maggiora, Physics of Plasmas **21**, p. 061507 (2014).
17. S. Ceccuzzi *et al.*, IEEE Trans. Antennas Propag. **62**, 5420–5424 (2014).
18. W. Tierens *et al.*, EPJ Web Conf. **157**, p. 03053 (2017).
19. R. Albanese *et al.*, Nuclear Fusion **57**, p. 016010 (2017).
20. V. Lancellotti *et al.*, Nuclear Fusion **46**, S476–S499 (2006).
21. D. Milanesio *et al.*, AIP Conference Proceedings **1406**, 81–84 (2011).
22. M. Brambilla, Plasma Physics and Controlled Fusion **31**, 723–757 (1989).
23. P. Lamalle, A. Messiaen, P. Dumortier, and F. Louche, Nuclear Fusion **46**, 432–443 (2006).